Turkish Journal of Electrical Engineering & Computer Sciences

http://journals.tubitak.gov.tr/elektrik/

Research Article

Turk J Elec Eng & Comp Sci
(2015) 23: 1930 – 1945

doi:10.3906/elk-1404-265

Frequency-adaptive grid-virtual-flux synchronization by multiple second-order generalized integrators under distorted grid conditions

Yingjie WANG[1,2], **Haiyuan LIU**[2,3], **Xuelong HAN**[2], **Kangan WANG**[2,*]

[1]Jiangsu Province Laboratory of Electrical and Automation Engineering for Coal Mining, China University of Mining and Technology, Xuzhou, P.R. China

[2]School of Information and Electrical Engineering, China University of Mining and Technology, Xuzhou, P.R. China

[3]College of Sciences, China University of Mining and Technology, Xuzhou, P.R. China

Received: 14.04.2014 • **Accepted/Published Online:** 09.07.2015 • **Printed:** 30.11.2015

Abstract: With some of the intermittent new energy and large nonlinear loads, grid voltage unbalance, harmonics, and frequency deviation are increasing year by year. The voltage source converter (VSC) is seriously affected by the various unexpected factors, and the presence of grid impedance makes the situation worse. In order to make the VSC track the nonideal grid quickly and accurately, this paper proposes a frequency-adaptive grid-virtual-flux synchronization by multiple second-order generalized integrators (MSOGI-GVFS). Key expressions of the MSOGI-GVFS and its frequency response characteristics are described in this paper. A second-order generalized integrator configured as a quadrature signal generator generates a specific-frequency virtual flux. A harmonics decoupling network achieves fundamental and harmonic components of the virtual flux. The positive- and negative-sequence components are separated by multiple positive- and negative-sequence calculators. A frequency-locked loop is used to track the grid angular frequency. Finally, after compensating the voltage and the flux on the grid impedance and the filtering inductor, it accurately achieves the estimation of the grid virtual flux in the highly polluted grid environment. This method may reduce the voltage sensors, eliminate the influence of grid impedance, and track the grid frequency quickly, which contributes to the stability of the VSC. The good performance of MSOGI-GVFS is verified by simulation and experimental results.

Key words: Grid virtual flux, second-order generalized integrator, harmonic decoupling network, frequency-locked loop, grid impedance, grid synchronization

1. Introduction

The voltage source converter (VSC) is emerging as the main topology of modular and standardized grid-connected converter units in a wide power range. A large variety of strategies for grid synchronization and control of VSCs have been proposed in the scientific literature [1–5]. Voltage-sensorless operation is among the topics that are gaining increasing interest for cost reduction, increased modularity, and eliminating the impedance of the power lines, which has a greater impact on VSCs [6,7]. Particularly in some remote grid applications, such as offshore wind power plants or photovoltaic power plants in high-altitude areas, grid impedance is large and the voltage-sensorless grid synchronization may have more applicability.

In the ideal grid, a phase-locked loop (PLL) [8] based on the synchronous reference frame can obtain satisfactory results. While the nonideal grid contains negative-sequence components and harmonic components,

*Correspondence: wyj971@126.com

this approach is unable to track the grid accurately. Using a notch filter or delayed signal cancellation filter [9] can extract the positive and negative sequence of the voltage fundamental component. However, these methods do not take the harmonic interference into consideration. There is also a fixed-frequency detection defect, so they cannot track very well when the grid frequency changes. The decoupled double synchronous reference frame PLL (DDSRF-PLL) [10] can detect fundamental negative-sequence components or the specified harmonic components, but when the DDSRF-PLL is extended in multiple reference frames, decoupling cells would be very complicated because feedback decoupling of each component uses a rotation transformation. Some scholars use the optimal iterative method with symmetrical components and state-space filter to approach the input signal [11,12]. Rodriguez et al. proposed a second-order generalized integrator-frequency-locked loop (SOGI-FLL) that makes improvements from an enhanced phase-locked loop by using the SOGI as the quadrature signal generator (QSG). This approach not only detects positive- and negative-sequence fundamental components of the grid, but it also takes low-order harmonics expansion into consideration [13]. This approach can also be adapted to the changes in the grid frequency.

The grid is very similar with the three-phase AC motor stator circuit. The DC bus voltage and switch states from the grid-connected VSC are used to construct and forecast the grid-virtual-flux vector as the orientation vector of the VSC [14,15], which has been the most popular grid synchronization without voltage sensors. However, this method has a problem with unknown initial values of its flux observations. If the fluxes are obtained by pure integrator, some DC bias associated with the integrated initial values is introduced to the estimation of the fluxes. In the literature [16,17], a practical improved method was proposed, using a low-pass filter instead of a pure integrator. However, this method is very sensitive to the changes in the grid frequency.

At present, grid synchronization based on grid virtual flux is mainly researched in the ideal grid. Under unbalanced grid conditions, the literature [18] first proposed a method where the low-pass filter is used to obtain virtual-flux-vector magnitude and a slower PLL is used to extract the positive frequency of the fluxes. The method, under synchronous reference frame, of joining the notch filter and low-pass filter to extract the positive-sequence components of the grid virtual fluxes was presented in the literature [19]. Cichowlas et al. [20] proposed a method using SDRF-PLL to detect the positive-sequence virtual fluxes. Kulka [21] proposed a method using a cascaded low-pass filter. In general, there are fewer studies that systematically applied grid synchronization based on grid virtual flux to the distorted and unbalanced grid.

From the literature above, three disadvantages about the current grid synchronization based on grid virtual flux can be summarized. First, the applied filters are sensitive to the changes in grid frequency. Second, under the unbalanced grid conditions, the methods have greater cascaded delay for obtaining flux and separating the positive- and negative-sequence work one after another. Third, there is no grid synchronization based on grid virtual flux under harmonic grid conditions.

To solve these problems, this paper proposes frequency-adaptive grid-virtual-flux synchronization by multiple second-order generalized integrators (MSOGI-GVFS). This approach integrates the estimation of the grid virtual flux with its subcomponent extraction by a harmonics decoupling network (HDN) containing SOGIs [22,23] and the multiple positive- and negative-sequence calculator (MPNSC). Thus, the fundamental and harmonic grid virtual fluxes are not only achieved correctly, but the transient response time is also reduced. The FLL [24] used in this approach can also follow the grid frequency. Finally, the simulation and experiment results verify the correctness and feasibility of this proposed approach.

2. Principle of the grid virtual flux estimation

Figure 1 shows the main structure of the grid-connected VSC. According to three-phase voltages on the point of common coupling (PCC), its control method adjusts the duty cycles to produce the converter side voltage. Voltage differences in the filter inductors are thereby achieved to produce the desired grid currents. At the same time, these duty cycles also control the DC bus current into the DC bus, which can produce the desired DC bus voltage. However, due to the grid impedance by which the grid currents would pass to absorb a part of the grid voltage, the voltages on the PCC are affected by the grid currents. If the grid impedance is large enough, it could seriously influence the performance of VSC. The stability of the grid-connected VSC can be analyzed by the impedance ratio and its Nyquist plot [25]. The impedance ratio can be expressed as:

$$F(s) = \frac{Z_g(s)}{Z_{oc}(s)}, \tag{1}$$

where Z_g (s) is the transfer function of the grid impedance. Z_{oc} (s) is the transfer function of the VSC output impedance including in the impedance of the controlling part.

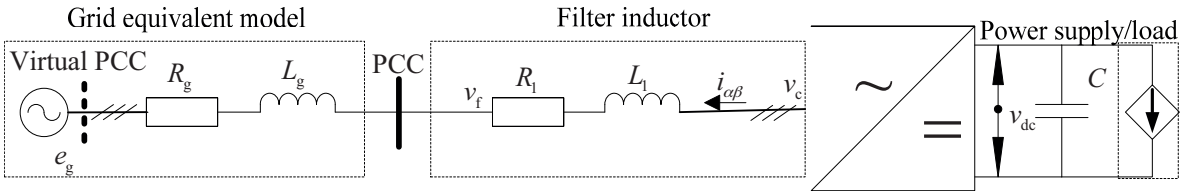

Figure 1. The main structure of grid-connected VSC.

As shown in Figure 2, the more the grid impedance decreases, the farther the Nyquist curve of the impedance ratio moves away from (-1,0), and the better the VSC's control performance is. If the voltages on the PCC are compensated with voltages on the grid impedance, grid voltages on the virtual PCC are obtained as a basis for the VSC control. Obviously, at this time, the grid impedance can be considered nonexistent, which will be very beneficial to improve the stability of the VSC. According to Figure 1, if the parameters of grid impedance and filter inductor are known, an equation to estimate grid voltages on the virtual PCC in two-phase stationary coordinates might be obtained as follows:

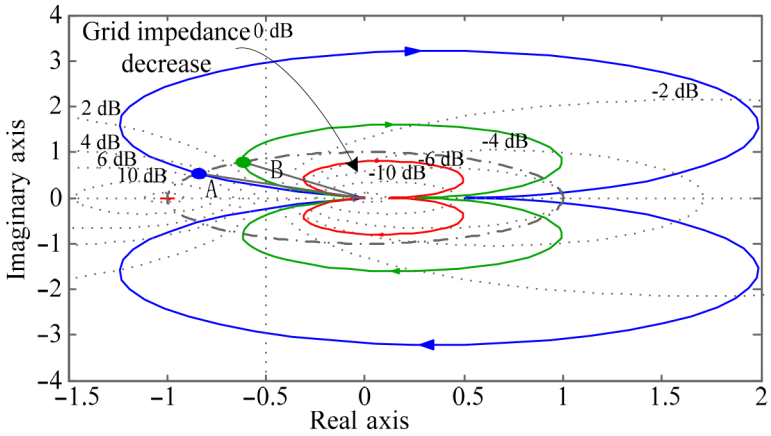

Figure 2. Nyquist plot of the impedance ratio.

$$e_{g,\alpha\beta} = v_{c,\alpha\beta} - R_z \cdot i_{g,\alpha\beta} - L_z \cdot \frac{di_{g,\alpha\beta}}{dt}, \tag{2}$$

where $e_{g,\alpha\beta}$ are grid voltages on the virtual PCC, $v_{c,\alpha\beta}$ are the output voltages of the VSC, and $i_{\alpha\beta}$ is the output current of the VSC. L_z and R_z respectively represent the total inductance and resistance on the filter inductor and the grid impedance. $v_{c,\alpha\beta}$ can be reconstructed by the DC bus voltage and the duty cycles of the switching device [26,27] just as Eq. (3) shows below:

$$\begin{cases} u_{c,\alpha} = \frac{2}{3}u_{dc}(S_a - \frac{1}{2}(S_b + S_c)) \\ u_{c,\beta} = \frac{\sqrt{3}}{3}u_{dc}(S_b - S_c) \end{cases}, \tag{3}$$

where S_a, S_b, and S_c represent the duty cycle of the a, b, and c phase bridge on the VSC, respectively. However, in Eq. (2), since the differential to the output current of the VSC is calculated, the current noises will be amplified to produce inaccurate estimation of grid voltages on the virtual PCC. Based on the principle of virtual flux, these noise interferences can be effectively avoided. The grid virtual fluxes on the virtual PCC can be expressed by [19,21]:

$$\psi_{g,\alpha\beta} = \int (v_{c,\alpha\beta} - R_z \cdot i_{g,\alpha\beta})dt - L_z \cdot i_{g,\alpha\beta}. \tag{4}$$

Introducing per unit values, the base values for voltage and flux are given by:

$$V_b = V_{phase} \quad V_{b,dc} = 2 \cdot V_b \quad \psi_b = \frac{V_b}{\omega_b} \quad P_b = 3.V_b.I_b. \tag{5}$$

Eq. (4) is rewritten as follows:

$$\psi^*_{g,\alpha\beta} = \omega_b \int (v^*_{c,\alpha\beta} - R^*_z \cdot i^*_{g,\alpha\beta})dt - L^*_z \cdot i^*_{g,\alpha\beta}. \tag{6}$$

This equation is an expression for ideal estimation of the grid virtual fluxes on the virtual PCC. Since the virtual flux corresponds to the integral of the voltage, its instantaneous phase angle lags behind the voltage phase angle by 90°. Therefore, the voltage phase angle θ_g can be easily estimated as given by:

$$\gamma_g = \arctan\left(\frac{\psi^*_{g,\beta}}{\psi^*_{g,\alpha}}\right) \quad \theta_g = \gamma_g + 90^\circ. \tag{7}$$

Since the integration required for virtual flux estimation implies a filtering effect, the instantaneous phase angle for synchronization can usually be calculated directly from Eq. (7). It can, of course, also be tracked by a PLL. Since the integrated initial values is unknown in Eq. (6), the DC bias will be introduced related to these values, resulting in inaccurate estimation. The conventional improved method is that the low-pass filter be replaced by the integrator, while compensating the phase or amplitude. There are two main ways, as shown in Figure 3. Figure 3a uses a first-order low-pass filter [28], which can only compensate the amplitude, while the filtering delay is longer. Figure 3b uses a cascaded low-pass filter [29], formed by plurality of a first-order low-pass filter. In this way not only can the amplitude be compensated, but the correct flux phase can also be achieved. However, two filters only adopt the fixed grid frequency and poor filtering capability, so they are only suitable for a strong grid. As for a weak grid, there may be larger grid-frequency fluctuation such that a big error would be the result.

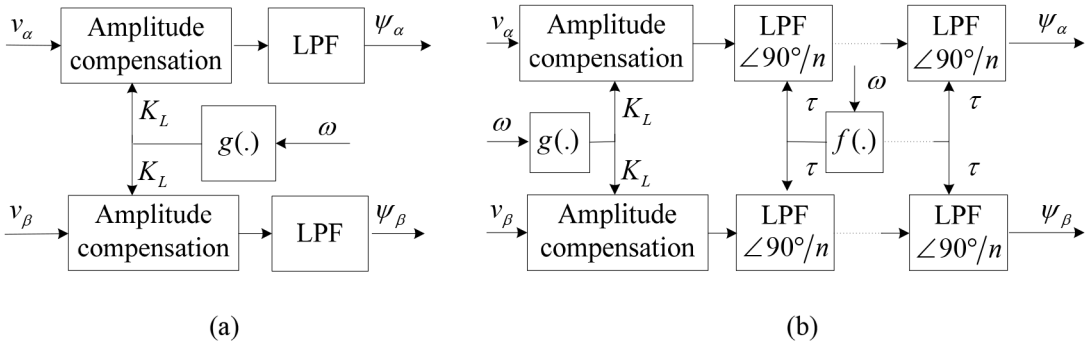

Figure 3. Two traditional flux observers: (a) based on a first-order low-pass filter, (b) based on a cascaded low-pass filter.

As for sinusoidal signal, a SOGI [12,13] can be configured as a frequency-adaptive band-pass filter and QSG by using feedback from the output signal. The resulting structure is shown in Figure 4. It is clearly seen that general voltage v with the various angular frequency and estimate ω' of the angular frequency are explicit inputs to the SOGI. The voltage signal with only the angular frequency ω' and its quadrature signal are explicit outputs from the SOGI. The transfer function of the filter from the input variable v to the filtered variable v' is given by:

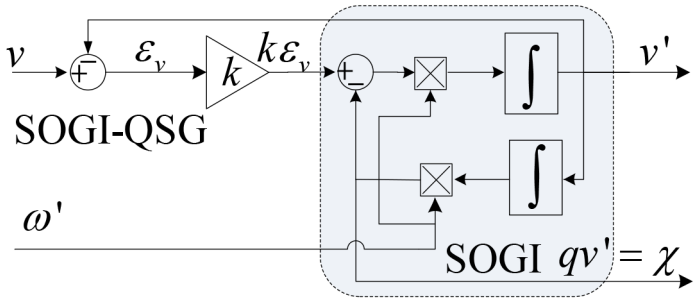

Figure 4. SOGI structure.

$$\frac{v'(s)}{v(s)} = \frac{k \cdot \omega' \cdot s}{s^2 + k \cdot \omega' \cdot s + \omega'^2}. \tag{8}$$

Eq. (8) corresponds to a critically second-order damped system. It can be seen that the frequency response can be adjusted by selecting the gain k. When k is equal to $\sqrt{2}$, this will be a good compromise between overshoot and settling time. Thus, $k = \sqrt{2}$ will be considered as the default value in the following discussion. In Figure 3, the quadrature output signal labeled as qv' is a value that the integral of the filtered output v' multiplies with the angular frequency ω', as given by

$$qv' = \omega' \int v'dt = \omega'_{pu} \cdot \omega_b \int v'dt = \chi. \tag{9}$$

With the reference to flux definition, the quadrature signal can be considered as per unit of flux signal, denoted by χ. By considering Eqs. (8) and (9), the transfer function of the quadrature output signal is given by

$$qv'(s) = \frac{k \cdot \omega'^2}{s^2 + k \cdot \omega' \cdot s + \omega'^2} v(s). \tag{10}$$

Eq. (10) corresponds to the second-order low-pass filter, which provides the unity gain and 90° phase shift for the input signal with the angular frequency ω'. According to Figure 4, the implementation of Eq. (10) will be inherently frequency-adaptive as long as the estimate of the grid angular frequency ω' is available. Combined with Eqs. (10) and (6), after compensating the resistance voltage and inductor flux, with the SOGI being the flux observer, the expression estimation of grid virtual flux is given by:

$$\psi^*_{g,\alpha\beta}(s) = \frac{k \cdot \omega'^2}{s^2 + k \cdot \omega' \cdot s + \omega'^2} \left[\left(v^*_{c,\alpha\beta}(s) - R^*_z \cdot i^*_{g,\alpha\beta}(s)\right)\right] - \omega'_{pu} \cdot L^*_z \cdot i^*_{g,\alpha\beta}(s). \tag{11}$$

This frequency information can, for instance, be provided by a PLL or by a FLL. The FLL's detailed structure is shown in Figure 5. The error signal $\varepsilon_{v(\alpha\beta)}$, output signal $v'_{\alpha\beta}$, and its quadrature signal $qv'_{\alpha\beta}$ from the SOGI are treated as FLL input signals. With reference to Eq. (11) and the FLL, it can get the grid virtual flux estimation method based on SOGI under balanced grid conditions, shown in Figure 6.

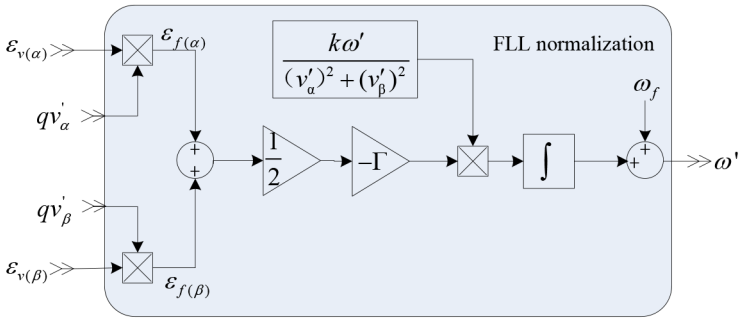

Figure 5. FLL's detailed structure.

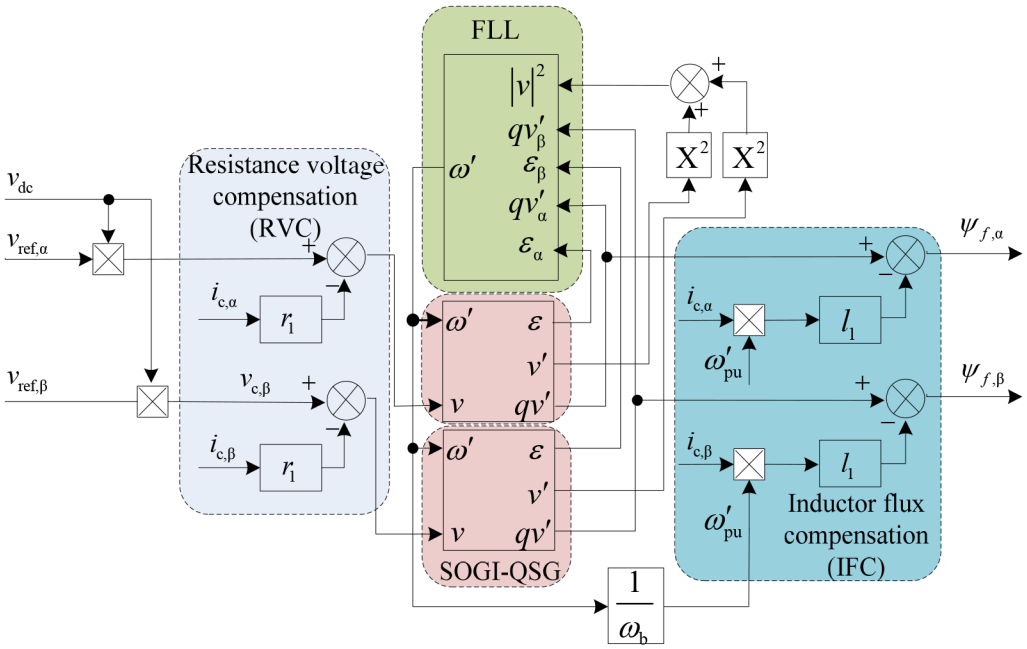

Figure 6. The grid virtual flux estimation method based on SOGI under balanced grid conditions.

3. Grid virtual flux estimation under unbalanced and distorted grid conditions

3.1. Under unbalanced grid conditions

In the unbalanced grid, the grid voltage contains a negative-sequence component, its vector locus is not a circle, and its vector rotation angular velocity changes, as shown in Figure 7. The positive- and negative-sequence components of the grid virtual fluxes as well as the grid frequency need to be separated. The positive- and negative-sequence calculator (PNSC) [30] may be used to directly separate the positive and negative sequence component of a signal, as shown in Eq. (12).

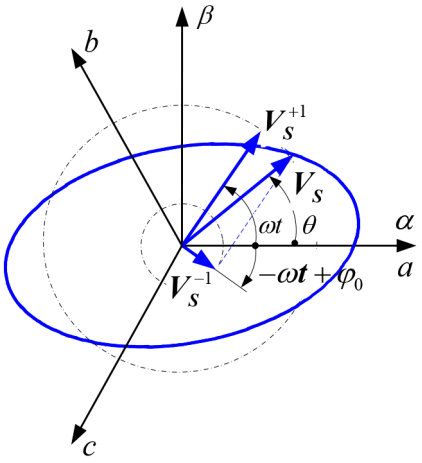

Figure 7. Unbalanced grid voltage vector locus.

$$\mathbf{v}_{\alpha\beta}^{+} = \frac{1}{2}\begin{bmatrix} 1 & -q \\ q & 1 \end{bmatrix}\mathbf{v}_{\alpha\beta}$$
$$\mathbf{v}_{\alpha\beta}^{-} = \frac{1}{2}\begin{bmatrix} 1 & q \\ -q & 1 \end{bmatrix}\mathbf{v}_{\alpha\beta} \tag{12}$$

In this equation, $q = e^{-j\pi/2}$ is a lagging phase shift operation. Taking into account that the SOGI quadrature output signal qv' represents a flux signal in Figure 4, a 90° backward signal to separate the positive- and negative-sequence components of a flux signal is needed. This signal can be obtained from the same SOGI filtered output signal v', which corresponds to $-q\chi$. Thus, the positive- and negative-sequence component of a flux signal can be gotten. Similarly, the same method can be used to isolate the positive- and negative-sequence components of the grid currents.

As shown in Figure 8, through the SOGI and PNSC, the fundamental fluxes are separated to their positive- and negative-sequence components. With the same method, the currents can also get their positive- and negative-sequence components. Then, after subtracting positive- and negative-sequence IFCs and RVCs, positive- and negative-sequence separation of grid virtual fluxes is finally achieved. It does not have the cascaded delay effect because obtaining the flux and separating the positive and negative sequences are almost simultaneous through the SOGI and PNSC.

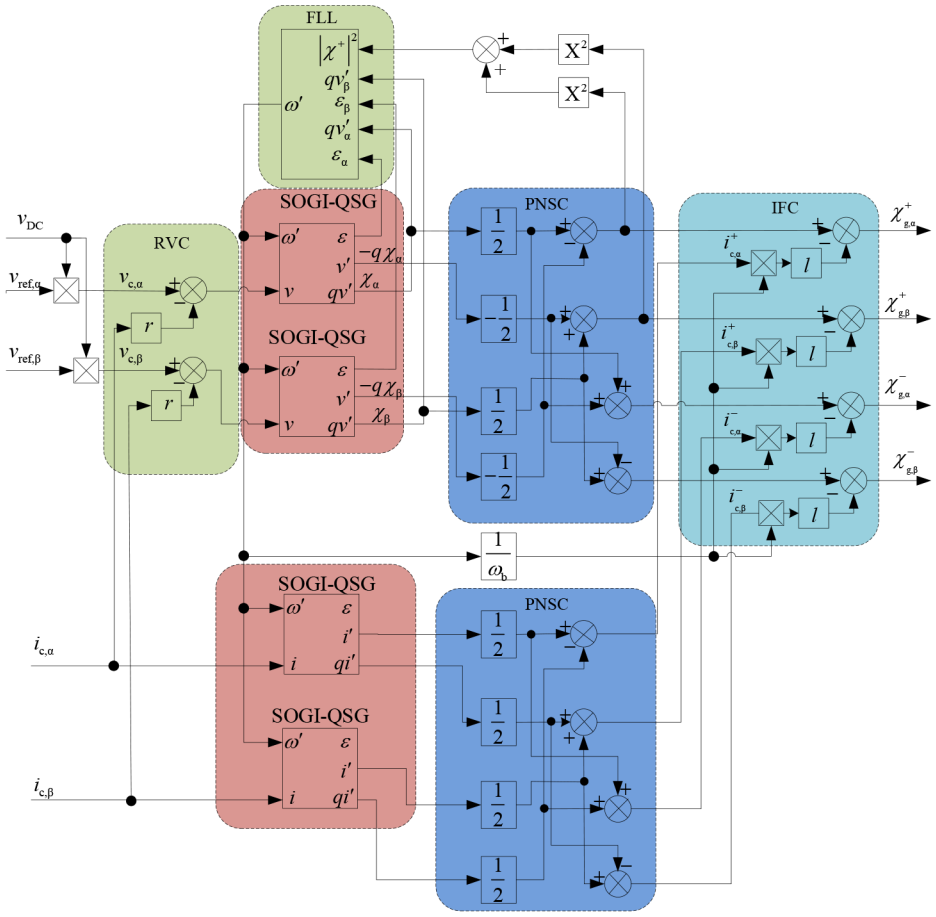

Figure 8. The grid virtual flux estimation based on SOGI under unbalanced grid conditions.

3.2. Under unbalanced and distorted grid conditions

The grid virtual flux estimation based on SOGI under unbalanced grid conditions discussed in Section 3.1 was introduced in [31]. This paper will further extend the virtual flux-based grid synchronization method to unbalanced and distorted grid conditions.

In the seriously distorted grid, a cross-feedback network consisting of multiple SOGI-QSGs with different filter frequencies can accurately detect the fundamental and harmonic components of the grid voltage, called the HDN [13] as shown in Figure 9. The HDN can be seen as a plurality of different adaptive filters with n selectable center frequencies in parallel pairs, named as DSOGI-QSG-i. That fundamental frequency detected by the FLL multiplied by the corresponding number of harmonics can adjust the frequency of the DSOGI-QSG-i. Therefore, it can detect the required harmonic components of the input signal. However, when the harmonic components are in a narrow band, detected results will be affected mutually. In order to avoid the influence, narrow bandwidth must be set in the DSOGI-QSG-i, but this in turn will cause additional transient shock to respond slowly. To avoid these problems, a cross-feedback network is used in the HDN. v_i is the input signal of a phase in DSOGI-QSG-i. $D_i(s)$ is the transfer function of the ith SOGI with reference to Eq. (8). The transfer function of the a-phase output signal v_i' of DSOGI-QSG-i is given by:

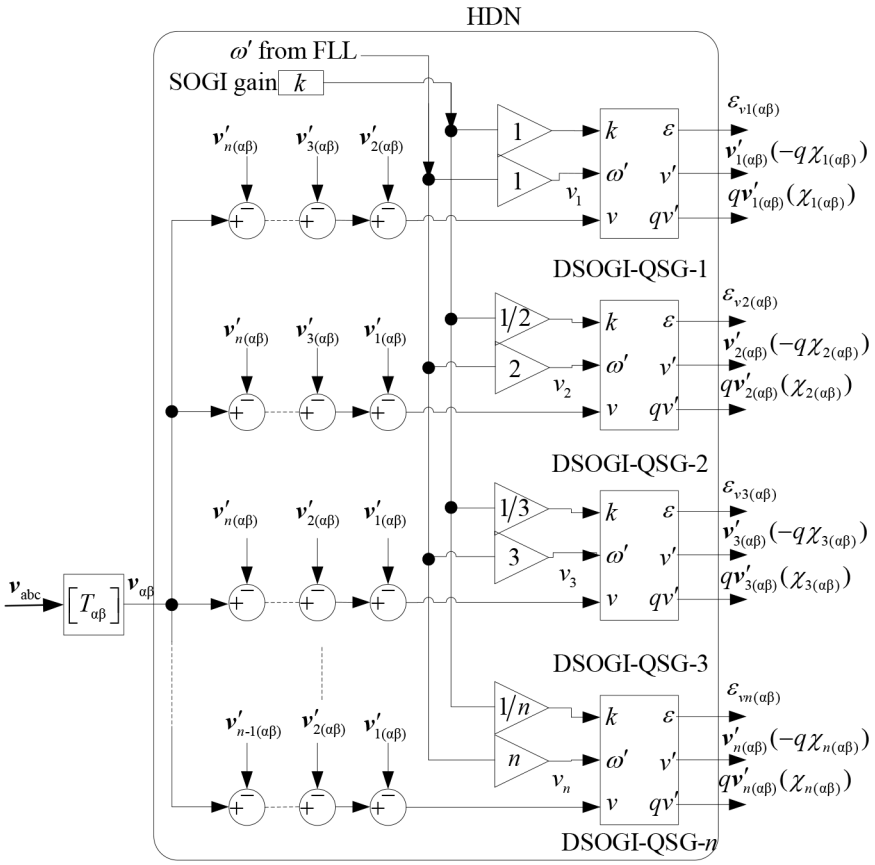

Figure 9. Harmonics decoupling network.

$$v_i' = D_i(s)\left(v - \sum_{\substack{j=1 \\ j\neq i}}^{n} v_j'\right). \tag{13}$$

After v_j' is obtained by the same method, the transfer function of the a-phase output signal v_i' of DSOGI-QSG-i can be further improved.

$$v_i' = \left[D_i(s)\prod_{\substack{j=1 \\ j\neq i}}^{n}\left(\frac{1-D_j(s)}{1-D_i(s)D_j(s)}\right)\right]v \tag{14}$$

Similarly, the transfer function qv_i' can be obtained with reference to Eqs. (10) and (14). As an example of the HDN effect, Figure 10 shows the Bode output signal passed by the HDN. The HDN comprises four DSOGI-QSGs and their center frequencies are 1st, 5th, 7th, and 11th harmonic frequencies, respectively. Center frequencies of the output signal in Figures 10a and 10b are respectively the 1st (50 Hz) and the 5th (250 Hz). The blue lines in Figures 10a and 10b are respectively their logarithmic frequency characteristic curves without a cross-feedback

network. The black lines in Figures 10a and 10b are respectively their logarithmic frequency characteristic curves with a cross-feedback network. As can be seen, the cross-feedback network generates a kerf at each SOGI-QSG center frequency. Thus, selective filtering characteristic of each SOGI-QSG are enhanced, and the response speeds of these DSOGI-QSGs may be improved for wider bandwidth.

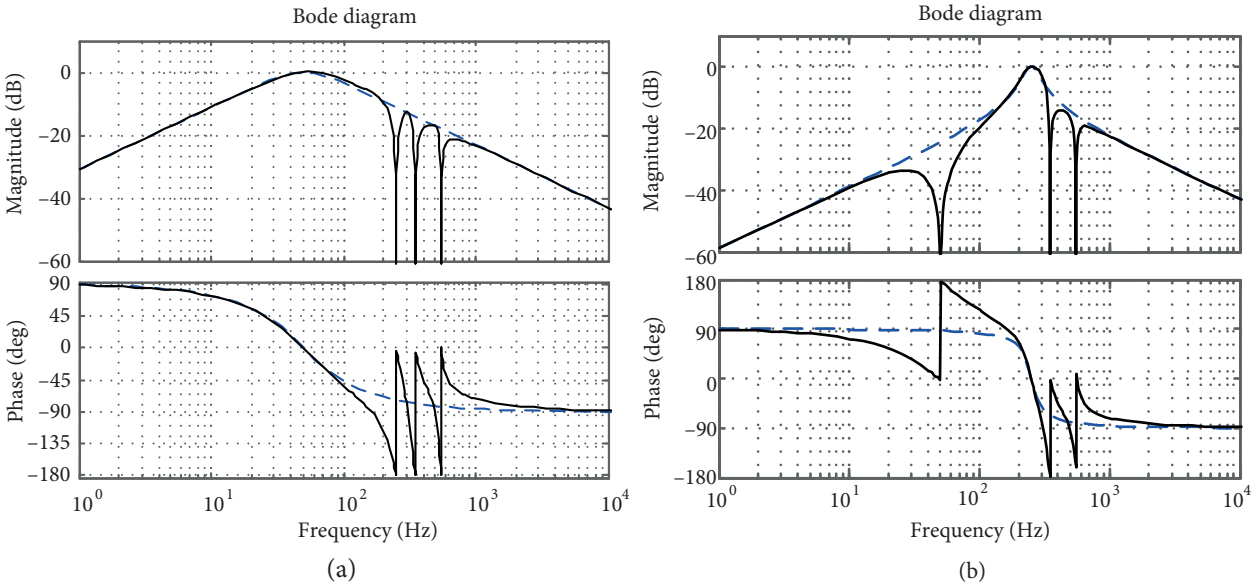

Figure 10. Bode diagram of output signal passed by HDN: (a) fundamental-frequency output signal, (b) fifth-frequency output signal.

The grid virtual flux estimation under unbalanced grid conditions has been discussed. However, when the grid is seriously distorted, due to the harmonics, the effect of the estimation will be greatly reduced. This paper presents a method called MSOGI-GVFS, as shown in Figure 11. After the resistance voltage compensation, each harmonic virtual flux corresponding to each harmonic voltage is decoupled by the HDN. The positive- and negative-sequence components of the virtual fluxes are got by the MPNSC. Therefore, the grid current may also be separated by the HDN and MPNSC. After positive- and negative-sequence IFCs, the grid virtual fluxes including in the positive- and negative-sequence components of n harmonics are finally obtained.

4. Simulation and experimental results

4.1. Simulation results

To test the transient response of the proposed method, an unbalanced and distorted grid fault is imposed to the system at 10 kVA at a 380-VRMS line voltage in MATLAB/Simulink. Its circuit structure is the same as in Figure 1. Grid impedance consists of L_g=0.03 pu and $R_g = 0.004$ pu. Filter inductor is 0.1 pu and its internal resistance 0.01 pu. At the beginning, a three-phase grid voltage phasor is balanced and set to $\mathbf{u}_{pf} = 1\angle 0^\circ$ pu. Its fundamental frequency is 50 Hz. With a fault in the grid at 0.2 s, its fundamental frequency is stepped down to 40 Hz. Fundamental positive- and negative-sequence phasors are $\mathbf{u}_{p1} = 0.5\angle -30^\circ$ pu and $\mathbf{u}_{n1} = 0.2\angle 110^\circ$ pu, respectively. For the 5th harmonic positive- and negative-sequence phasor, $\mathbf{u}_{p5} = 0.15\angle 135^\circ$ pu and $\mathbf{u}_{n5} = 0.1\angle 45^\circ$ pu. For the 7th harmonic positive- and negative-sequence phasor, $\mathbf{u}_{p7} = 0.1\angle 15^\circ$ pu and $\mathbf{u}_{n7} = 0.2\angle 0^\circ$ pu. The center frequency of DSOGI-QSG-1 is the fundamental frequency for the FLL and the gain $k_1 = \sqrt{2}$. The remaining DSOGI-QSG-i gain is set by the gain k_1 divided by corresponding number of

harmonics for making all the DSOGI-QSGs have the same filtering characteristic. Finally, FLL gain is $\Gamma = 50$. The simulation results of the grid virtual flux estimation are shown in Figure 12.

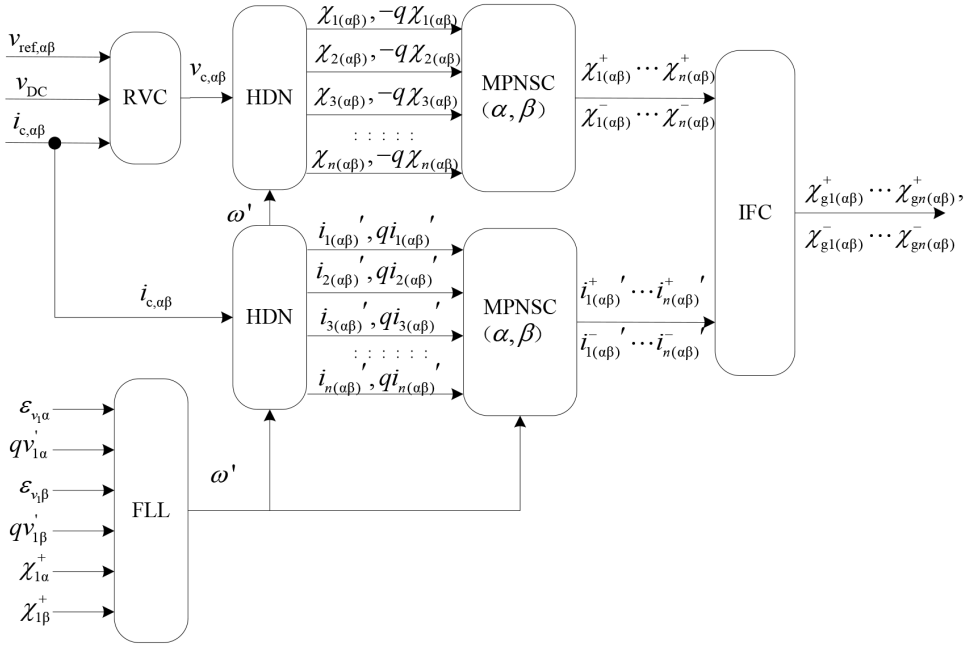

Figure 11. MSOGI-GVFS under unbalanced and distorted grid conditions.

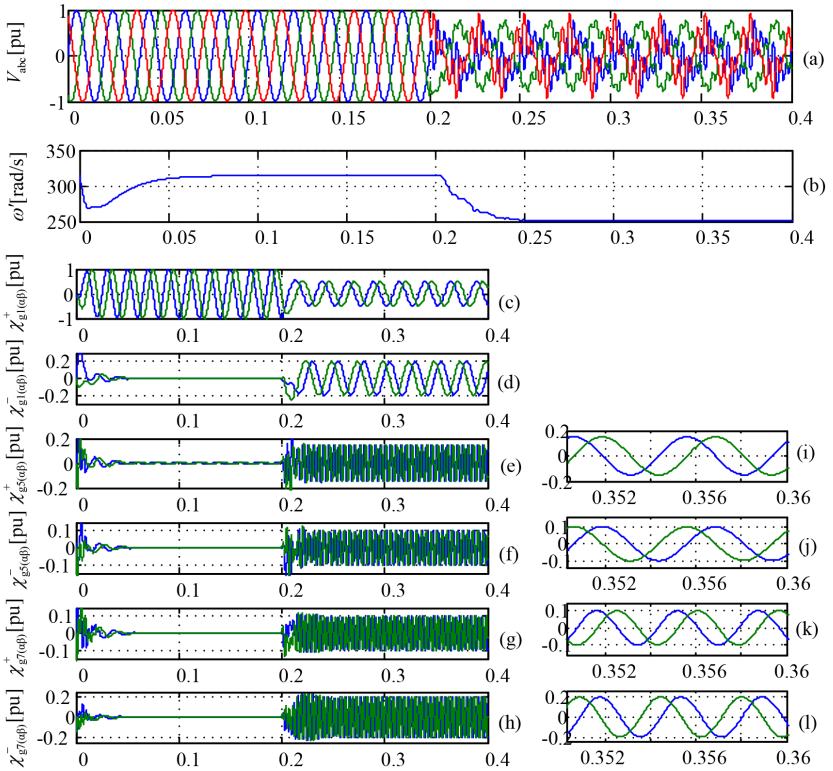

Figure 12. The simulation results of the grid virtual flux estimation.

Figure 12a shows the three-phase grid-voltage waveform before and after the grid fault. It can be seen that a serious unbalance and distortion and hopping appeared in the grid voltage after 0.2 s. Figure 12b shows the grid fundamental frequency detected by the FLL, from which it can be seen that the FLL can achieve good adaptivity. As can be seen from Figures 12c–12h, positive- and negative-sequence components of the grid fundamental and 5th and 7th harmonic virtual fluxes are estimated accurately and quickly. Figures 12i–12l are the enlarged views of Figures 12e–12h.

Figures 13a–13f are positive- and negative-phase tracking charts of the grid fundamental and 5th and 7th harmonic virtual fluxes and grid voltages. All the virtual flux phase estimations lag behind the corresponding voltage phase by 90°, which achieves the purpose of tracking the grid phase and proves the correctness of virtual flux estimation.

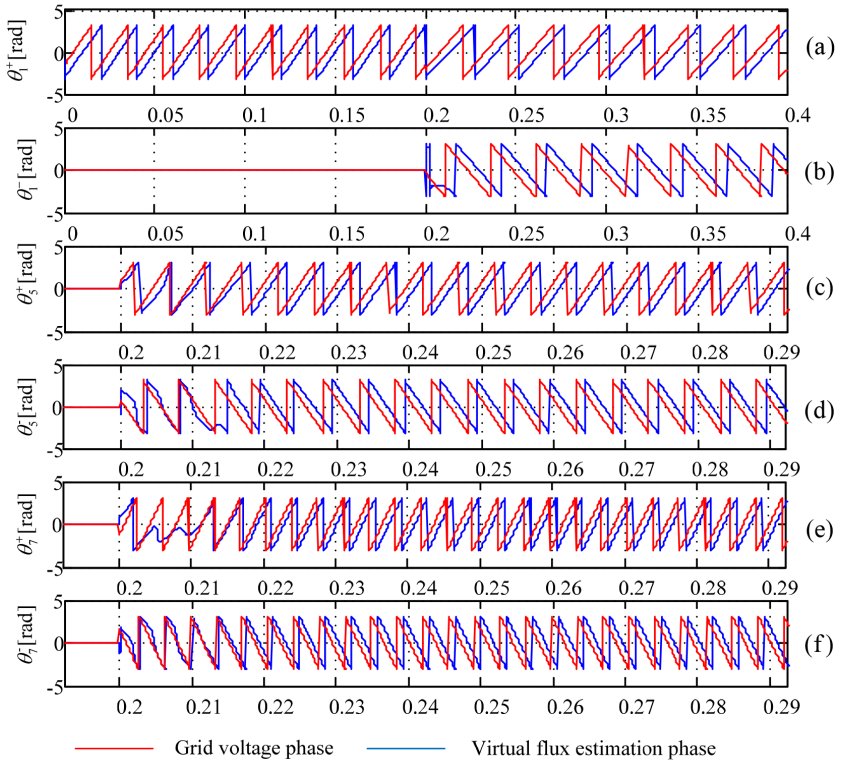

Figure 13. Phase tracking chart of the grid fundamental and 5th and 7th harmonic virtual fluxes and grid voltages.

4.2. Experimental results

To further validate the correctness of the method, a 1.8-kW three-phase voltage generator is established to analog the unbalanced and distorted grid, as shown in Figure 14. The grid virtual flux estimation is achieved with dSPACE 1104 with L_g and R_g analog grid impedance. The Table shows the parameters of the experimental system.

The amplitude of the fundamental positive-sequence component is 0.3 pu, the amplitude of the fundamental negative-sequence component is 0.1 pu, the amplitude of the 5th harmonic positive-sequence component is 0.1 pu, the amplitude of the 5th harmonic negative-sequence component is 0.1 pu, the amplitude of the 7th harmonic positive-sequence component is 0.1 pu, and the amplitude of the 7th harmonic negative-sequence component is 0.05 pu. Figure 15 shows the experimental results. Cursor 1 represents the per-unit value of the

A-phase detected current (1 pu: 0.5 V). Cursor 2 is the per-unit value of the A-phase detected voltage (1 pu: 1 V). Cursor 3 is the fundamental angular frequency (1 rad/s: 1.5 mV). Cursor 4 is the per-unit value of the α-axis grid virtual flux of the fundamental positive-sequence component estimated by MSOGI-GVFS (1 pu: 0.5 V). Figure 15a shows the response waveforms when the MSOGI-GVFS is starting. Figure 15b shows the steady-state response waveforms. Figure 15c shows the response waveforms of the fundamental frequency from 50 Hz to 45 Hz mutation. Figure 15 shows that MSOGI-GVFS has a good adaptive performance and can track the changes of the grid quickly.

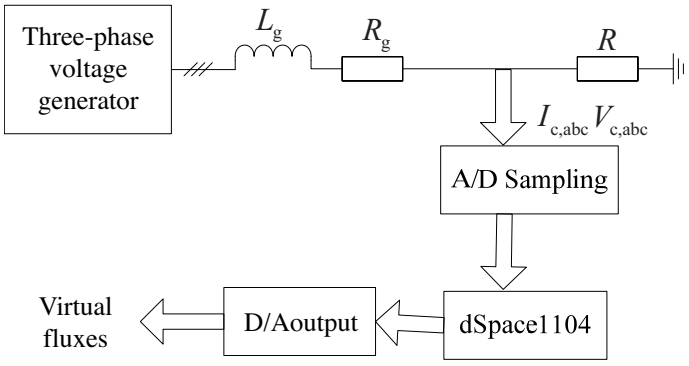

Figure 14. Experimental system block diagram.

Table. Parameters of the experimental system.

Parameters	Unit	Value
Rated power	kW	1.8
Fundamental frequency	Hz	50
Sampling frequency	kHz	10
Rated voltage	V	110
Line resistance	Ω	0.2
Line inductance	mH	5
Filter capacitor	μF	4.6 (Δ type)
Load	Ω	20

5. Conclusions

In this paper, a new synchronization method, MSOGI-GVFS, under unbalanced and distorted grid conditions is proposed. First, in order to raise frequency adaptivity and filtering capability, the SOGI as a basic framework module is used in this synchronization method. The SOGI and PNSC are integrated to realize the specific-frequency virtual fluxes and their positive and negative sequences simultaneously without cascade delay. The HDN included in the cross-feedback network and multiple SOGI-QSGs achieves the decoupling of each harmonic virtual flux as well as each harmonic voltage. The cross-feedback network enhances selective filtering characteristics and the response speed of each SOGI-QSG. Thus, MSOGI-GVFS has a high-damping fast transient response. Then IFCs and RVCs achieve estimation of the grid virtual fluxes on a virtual PCC by compensating voltages and fluxes on the grid impedance and filtering inductor. The grid virtual fluxes on the virtual PCC are obtained to provide a foundation that improves the stability of the VSC. Since MSOGI-GVFS contains the FLL, used to detect the fundamental frequency of the input signal, the system has a frequency-adaptive function. The simulation and experimental results show that MSOGI-GVFS can still quickly and accurately detect the

fundamental-frequency and harmonic-frequency positive- and negative-sequence grid virtual flux components when even the grid suffers from extreme pollution. These results also prove the correctness of the theoretical analysis and the feasibility of the proposed method.

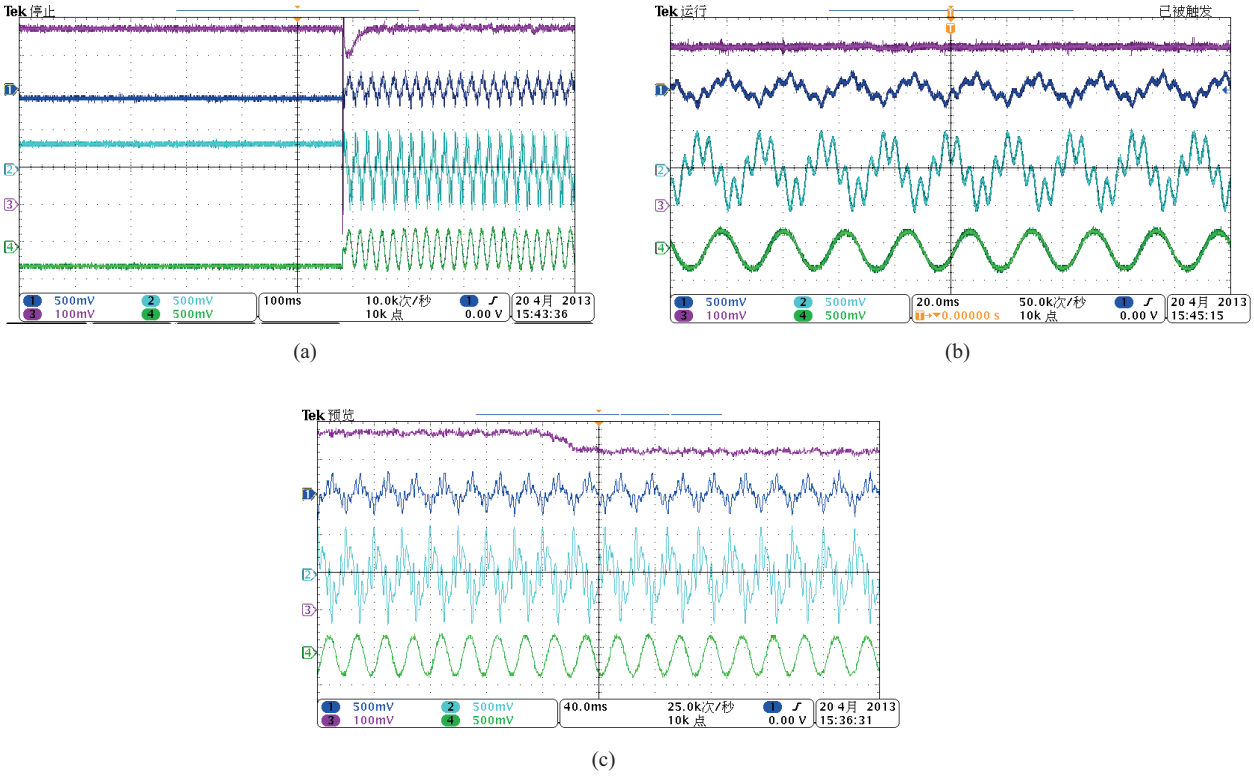

Figure 15. Experimental results.

Acknowledgments

The authors would like to give thanks for project support by the Specialized Research Fund for the Doctoral Program of Higher Education (20120095110017), the China Postdoctoral Science Foundation (2014M561726), the Laboratory Construction Program for the Mining Electrics and Automation in Jiangsu Province (2014KJZX05), and the National Natural Science Foundation of China (51377160).

References

[1] Blaabjerg F, Teodorescu R, Liserre M, Timbus AV. Overview of control and grid synchronization for distributed power generation systems. IEEE T Ind Electron 2006; 53: 1398–1409.

[2] Kazmierkowski MP, Malesani L. Current control techniques for three-phase voltage-source PWM converters: a survey. IEEE T Ind Electron 1998; 45: 691–703.

[3] Ghartemani MK, Iravani MR. A method for synchronization of power electronic converters in polluted and variable-frequency environments. IEEE T Power Syst 2004; 19: 1263–1270.

[4] Timbus V, Liserre M, Teodorescu R, Blaabjerg F. Synchronization methods for three phase distributed power generation systems. An overview and evaluation. In: Power Electronics Specialists Conference; Recife, Brazil; 2005. New York, NY, USA: IEEE. pp. 2474–2481.

[5] Timbus A. Grid Monitoring and Advanced Control of Distributed Power Generation Systems. Aalborg, Denmark: Aalborg University, 2007.

[6] Noguchi T, Tomiki H, Kondo S. Direct power control of PWM converter without power- source voltage sensors. IEEE T Ind Appl 1998; 34: 473–479.

[7] Suul JA, Undeland T. Flexible reference frame orientation of virtual flux-based dual frame current controllers for operation in weak grids. In: Proceedings of PowerTech; Trondheim, Norway; 2011. New York, NY, USA: IEEE. pp. 1–8.

[8] Chung S. A phase tracking system for three phase utility interface inverters. IEEE T Power Electr 2000; 15: 431–438.

[9] Saccomando G, Svensson J. Transient operation of grid-connected voltage source converter under unbalanced voltage conditions. In: Industry Applications Conference; 2001. New York, NY, USA: IEEE. pp. 2419–2424.

[10] Rodriguez P, Pou J, Bergas J, Candela J, Burgos RP, Boroyevich D. Decoupled double synchronous reference frame PLL for power converters control. IEEE T Power Electr, 2007; 22: 584–592.

[11] Karimi-Ghartemani M, Karimi H. Processing of symmetrical components in time-domain. IEEE T Power Syst 2007; 22: 572–579.

[12] Rodriguez P, Luna A, Ciobotaru M, Teodorescu R, Blaabjerg F. Advanced grid synchronization system for power converters under unbalanced and distorted operating conditions. In: IECON 32nd Annual Conference on Industrial Electronics; Paris, France; 2006. New York, NY, USA: IEEE. pp. 5173–5178.

[13] Rodriguez P, Alvaro L, Ignacio C, Ramon M, Remus T, Frede B. Multiresonant frequency-locked loop for grid synchronization of power converters under distorted grid conditions. IEEE T Power Electr 2011; 28: 127–138.

[14] Hailian X, Angquist L, Nee H. Comparison of voltage and flux modulation schemes of STATCOMs regarding transformer saturation during fault recovery. IEEE T Power Syst 2008; 23: 1653–1661.

[15] Kwon BH, Youm JH, Lim JW. A line-voltage-sensorless synchronous rectifier. IEEE T Power Electr 1999; 14: 966–972.

[16] Suul JA, Luna A, Rodriguez P, Undeland T. Voltage-sensor-less synchronization to unbalanced grids by frequency-adaptive virtual flux estimation. IEEE T Ind Electron 2012; 59: 2910–2923.

[17] He Z, Liao Y, Xiang D. A new flux estimation method based on modified programmable cascaded low-pass filter. Transactions of China Electrotechnical Society 2008; 24: 53–58.

[18] Malinowski M, Marques G, Cichowlas M, Kazmierkowski MP. New direct power control of three-phase PWM boost rectifiers under distorted and imbalanced line voltage conditions. In: 2003 IEEE International Symposium on Industrial Electronics; 2003. New York, NY, USA: IEEE. pp. 438–443.

[19] Jasinski M, Okon P, Kazmierkowski MP. Control of grid-interfacing AC-DC-AC converter for variable speed energy generation under unbalanced and distorted voltage conditions. In: Proceedings of Compatibility and Power Electronics; Monaco; 2009. pp. 139–145.

[20] Cichowlas M, Malinowski M, Kazmierkowski MP, Sobczuk DL, Rodriguez P, Pou J. Active filtering function of three-phase PWM boost rectifier under different line voltage conditions. IEEE T Ind Electron 2005; 52: 410–419.

[21] Kulka A. Sensorless digital control of grid connected three phase converters for renewable sources. PhD, Norwegian University of Science and Technology, Trondheim, Norway, 2008.

[22] Matas J, Castilla M, Miret J, Garcia de Vicuna L. An adaptive prefiltering method to improve the speed/accuracy tradeoff of voltage sequence detection methods under adverse grid conditions. IEEE T Ind Electron 2014; 61: 2139–2151.

[23] Alfonso-Gil JC, Vague-Cardona JJ, Orts-Grau S, Gimeno-Sales FJ, Segui-Chilet S. Enhanced grid fundamental positive-sequence digital synchronization structure. IEEE T Power Deliver 2013; 28: 226–234.

[24] Vazquez S, Sanchez JA, Reyes MR, Leon JI, Carrasco JM. Adaptive vectorial filter for grid synchronization of power converters under unbalanced and/or distorted grid conditions. IEEE T Ind Electron 2014; 61: 1355–1367.

[25] Huang J, Corzine KA, Belkhayat M. Small-signal impedance measurement of power-electronics- based ac power systems using line-to-ling current injection. IEEE T Power Electr 2009; 24: 445–455.

[26] Malinowski M, Kazmierkowski MP, Hansen S, Blaabjerg F, Marques GD. Virtual-flux-based direct power control of three-phase PWM rectifiers. IEEE T Ind Appl 2001; 37: 1019–1027.

[27] Malinowski M, Jasiński M, Kazmierkowski MP. Simple direct power control of three-phase PWM rectifier using space vector modulation (DPC-SVM). IEEE T Ind Electron 2004; 51: 447–454.

[28] Pöllänen R. Converter-flux-based current control of voltage source PWM rectifiers—Analysis and implementation. PhD, Lappeenranta University of Technology, Lappeenranta, Finland, 2003.

[29] Bose B, Patel N. A programmable cascaded low-pass filter based flux synthesis for a stator flux oriented vector controlled induction motor driveIEEE T Ind Electron 1997; 44: 140–143.

[30] Chaudhary SK, Teodorescu R, Rodriguez P, Kjaer PC, Gole AM. Negative sequence current control in wind power plants with VSC-HVDC connection. IEEE T Sustain Energ 2012; 3: 535–544.

[31] Suul JA. Control of grid integrated voltage source converters under unbalanced conditions - development of an on-line frequency adaptive virtual flux-based approach. PhD, Norwegian University of Science and Technology, Trondheim, Norway, 2012.